

From Raw Data to Structural Semantics: Trade-offs among Distortion, Rate, and Inference Accuracy

Charmin Asirimath, Chathuranga Weeraddana, Sumudu Samarakoon, *Member, IEEE*, Jayampathy Ratnayake, and Mehdi Bennis, *Fellow, IEEE*

Abstract—This work explores the advantages of using persistence diagrams (PDs), topological signatures of raw point cloud data, in a point-to-point communication setting. PD is a structural semantics in the sense that it carries information about the shape and structure of the data. Instead of transmitting raw data, the transmitter communicates its PD semantics, and the receiver carries out inference using the received semantics. We propose novel qualitative definitions for distortion and rate of PD semantics while quantitatively characterizing the trade-offs among the distortion, rate, and inference accuracy. Simulations demonstrate that unlike raw data or autoencoder (AE)-based latent representations, PD semantics leads to more effective use of transmission channels, enhanced degrees of freedom for incorporating error detection/correction capabilities, and improved robustness to channel imperfections. For instance, in a binary symmetric channel with nonzero crossover probability settings, the minimum rate required for Bose, Chaudhuri, and Hocquenghem (BCH)-coded PD semantics to achieve an inference accuracy over 80% is approximately $15\times$ lower than the rate required for the coded AE-latent representations. Moreover, results suggest that the gains of PD semantics are even more pronounced when compared with the rate requirements of raw data.

Index Terms—persistence diagram (PD), semantic communication, semantic distortion, semantic rate, trade-offs

I. INTRODUCTION

The study of *semantics*, from a communication theory standpoint, dates back to Weaver and Shannon in 1949 [1]. Back then, the communication problem was discussed in three levels: Levels A, B, and C, which correspond to the technical problem, semantic problem, and effectiveness problem, respectively [1, p 4]. The technical problem (level A) is based on the mathematical theory of communication introduced by Claude E. Shannon [1, p 29], [2]. Subsequently, contemporary related research by Bar-Hillel and Carnap [3]–[5] argues for the need for new mathematical formulations toward the semantic problem (level B), indicating the limitations of the theories at level A are due to the statistical nature of information. Since then, the literature has not shown much progress for around seven decades in terms of engineering communication systems until the recent advancements in machine learning (ML). The envisioned futuristic communication system requirements,

Charmin Asirimath is with School of Computing, University of Eastern Finland, Finland (e-mail: charmin.pingamage.don@uef.fi). Chathuranga Weeraddana, Sumudu Samarakoon, and Mehdi Bennis are with Centre for Wireless Communication, University of Oulu, Finland (e-mail: chathuranga.weeraddana@oulu.fi, sumudu.samarakoon@oulu.fi, and mehdi.bennis@oulu.fi, respectively). Jayampathy Ratnayake is with the Department of Mathematics, University of Sri Jayewardenepura, Sri Lanka (e-mail: jratnayake@sjp.ac.lk).

together with modern ML techniques have paved the way for deep insights into computationally extracting semantics from raw data for downstream tasks [6]–[8]. As a result, there has been an unprecedented interest in goal-oriented and semantic communication [9]–[15].

Computational frameworks for extracting semantics from raw data for goal-oriented communications are typically based on ML models leveraging information-theoretic frameworks or explicit schemes that yield *structural attributes* of the underlying data. More specifically, ML-based semantics are usually extracted based on classic rate-distortion (RD) [16], and the framework of information bottleneck (IB) [17]. On the other hand, for structure-based techniques, there is a growing interest in integrating topological signatures of data in various downstream tasks [18], which in turn suggests their use in goal-oriented communication. In this respect, persistence homology (PH) is a powerful tool for capturing topological structures of the data [18, § 5]. As such, persistence diagrams (PDs) [18, § 5.3] as a summary of PH, provide topological signatures of great importance for ML applications [18]–[29].

Unlike ML-based semantics, structural semantics such as PDs originating from topological primitives have not been explored in terms of their associated trade-offs in a goal-oriented semantic communication system. However, the need for such a study, either theoretical or empirical is of paramount importance and is the main focus of this paper.

A. Related Work

In general, methods for extracting semantic attributes from raw data for goal-oriented communication are divided into two types: those derived from ML algorithms [30]–[41] and those based on explicit data/information structures [42]–[49]¹. ML-based semantic extraction heavily depends on information theoretic primitives such as classic RD and the framework of IB, *cf.* [30]–[34] and [35]–[41], respectively. Unlike the ML-based semantic extraction methods, techniques for extracting structural semantics of raw data are diverse. However, applications of such techniques in goal-oriented semantic communication are yet to be investigated. In the sequel, we discuss in detail the literature related to these two types for extracting semantic attributes from raw data.

¹There are specific semantic attributes for which the extraction mechanisms may not directly align with the previously mentioned types. For instance, the semantics of ‘freshness’, ‘relevance’, and ‘value’ within the semantic-aware communication architecture proposed for networked control systems [50] place a greater emphasis on timeliness and sampling of raw data.

ML-based Semantic Extraction:

In formulations based on classic RD [30]–[34], it is commonplace to study problems using natural language processing (NLP) (e.g., [30], [31]) or nonlinear transform coding (NTC) (e.g., [32], [33]) that are implemented via neural networks (NNs). In certain cases, additional NNs are employed to map semantics to channel symbols yielding a joint source and channel coding (JSCC) setup [30], [32], [33]. Considered distortions are usually measured in the raw data space by using a cross-entropy model and the rates are measured by using appropriately chosen entropy models. For instance, maps from images to semantics and semantics to images considered in [34] are based on an autoencoder (AE), and the distortion is measured in raw data space. However, unlike the methods in [30]–[33], [34] implements quantization based on dedicated NNs that account for the desired rate requirements.

The other class of ML-based semantics is based on the IB framework originally proposed in [17]. In a broader sense, the framework of IB enables a minimal representation with a maximal informativeness of some target variable using raw source data. The minimality accounts for complexity, an indication of the rate or the number of bits required to encode the representation. On the other hand, the maximality accounts for the relevance of the representation to the target variable. Consequently, there is a trade-off between informativeness and rate requirements of the resulting representation. Recently, there has been a growing interest in these semantics within the context of goal-oriented communication [35]–[41].

It is worth highlighting that ML-based models [30]–[41] intrinsically characterize the trade-offs among rate, distortion, and informativeness, since the models are governed by underlying information theoretic frameworks, such as classic RD and IB frameworks.

Data/Information Structures-based Semantic Extraction:

Extracting structural semantics from data is a multifaceted process that involves a combination of topology [18], graph theory [44], clustering [51], dimensionality reduction methods [52], logical formulations [53], and causal structures [54]. However, the research toward investigating the potential benefits of the choice of structural semantics is still at a very early stage [15, § II-A]. As pointed out in [13, § II-B], knowledge graphs have been used in recent literature highlighting their abilities to extract semantics from raw data, *cf.* [42]–[45]. Another graph-based representation of raw data that is closely related to the knowledge graph is proposed in [46]. Authors in [47] and [48] have used a mechanism to map raw data into simplicial complexes, an algebraic structure, to be used in inference tasks. The authors of [49] present a mechanism for extracting causal structures in the context of goal-oriented semantic communication.

It is worth pointing out that, in contrast to the ML-based semantic extraction, trade-offs among rate, distortion, and informativeness have not been investigated in the case of structural semantics [42]–[47], [49], despite their importance in goal-oriented communication system design standpoint.

B. Motivation and Contribution

Similar to the structural semantics proposed in [42]–[49], topological signatures such as PDs have shown unprecedented potential in modern ML application domains, but have not been considered so far in semantic communication [18]–[29]. The proliferation of PDs in application domains is emphasized further by the recent research conducted to develop dedicated ML architectures for handling PDs as inputs [19]–[23].

However, the potential of PDs as structural semantics in the paradigm of goal-oriented communication is yet to be explored. In this respect, there is a need to investigate trade-offs among *distortion*, *rate requirement*, and *inference accuracy* in a system where PDs are used as semantics, which we refer to as PD semantics. As such, the key contributions of the paper are summarized below:

- *Benefits of PD Semantics:* Conduct a study to explore the advantages of using PDs as structural semantics over raw data and AE-latent representations in a point-to-point goal-oriented communication setting.
- *Communication of Semantics:* Propose strategies for transmitting PD semantics from a transmitter (e.g., sensor) to a receiver (e.g., a central node).
- *Qualitative Definitions:* Develop qualitative definitions for semantic distortion and rate within the scope of PDs.
- *Quantitative Characterization:* Characterize quantitatively the trade-offs among the distortion, the rate, and inference accuracy for a downstream task of interest.
- *Empirical Evidence:* Empirically demonstrate that PD semantics offer significant advantages over raw data and AE-latent representations including:
 - Effective use of transmission channels.
 - Provisioning additional error detection/correction capabilities for enhanced robustness against communication channel impairments.
 - Robustness of the inference to changes in the distortion and the rate.

C. Notation

Normal font lowercase letters x , bold font lowercase letters \mathbf{x} , and calligraphic font \mathcal{X} represent scalars, vectors, and sets, respectively. The transpose of a vector \mathbf{x} is represented by \mathbf{x}^T . The sets of real numbers, natural numbers, and real n -vectors are denoted by \mathbb{R} , \mathbb{N} , and \mathbb{R}^n , respectively. We denote the Euclidean distance and maximum norm by $\|\mathbf{x}\|_2$ and $\|\mathbf{x}\|_\infty$, respectively. The nonnegative orthant \mathbb{R}_+^n is the set of points with nonnegative components, i.e., $\mathbb{R}_+^n = \{\mathbf{x} \in \mathbb{R}^n \mid x_i \geq 0, i = 0, \dots, n\}$. The simplex spanned by a list of vectors $\mathbf{x}_0, \dots, \mathbf{x}_n$ is denoted by $[\mathbf{x}_0, \dots, \mathbf{x}_n]$.

D. Organization of the Paper

The rest of the paper is organized as follows. The related background is concisely presented in Section II. The system model and problem statement are presented in Section III. In Section IV, we present a novel approach for transmitting PD semantics. Section V defines the notion of semantic distortion and semantic rate, which are used in our subsequent empirical

characterizations and associated trade-offs. In Section VI, empirical characterizations of trade-offs and their implications are presented. Lastly, Section VII concludes the paper.

II. BACKGROUND

In this section, we outline the mathematical concepts and tools used in this paper for generating PD semantics of raw point cloud data, *cf.* § II-A and II-B. Moreover, a machinery for adapting PDs as inputs for NNs is presented in § II-C.

A. Point Clouds

A point cloud \mathcal{G} is a set of points that reside in an ambient space, usually the Euclidean space, while each point in the point cloud encodes certain information about the underlying space. From an engineering point of view, sensor technologies including Light Detection and Ranging (LiDAR), cameras, and structured light cameras are capable of generating such point clouds. In the technical problem (level A) systems, it is commonplace that such sensors routinely transmit their point cloud to a remote server or receiver. However, transmitting the entire point cloud requires significant resources. In contrast, we propose a novel approach based on communicating a topological signature that encodes topological attributes underlying the point cloud, allowing more efficient communication for solving downstream tasks.

B. An Overview of PH

In this subsection, we introduce the necessary mathematical tools for generating a signature that encodes the topological structure of the point cloud. For more details, we refer the reader to [55].

1) *Simplices and Simplicial Complexes:* We start by first introducing the mathematical object called *simplices*, which are generalizations of the notion of a triangle to an arbitrary dimension. Loosely speaking, a 0-simplex is a point in Euclidean space, a 1-simplex is a line segment, a 2-simplex is a filled triangle, a 3-simplex is a filled tetrahedron, and the concept is generalized similarly for higher order simplices. Formally, a k -simplex denoted σ is defined as

$$\sigma = \left\{ \sum_{i=0}^k \theta_i \mathbf{u}_i \mid \sum_{i=0}^k \theta_i = 1, \theta_i \geq 0, i = 0, \dots, k \right\}, \quad (1)$$

where $\mathbf{u}_0, \dots, \mathbf{u}_k$ are affinely independent points in d dimensional Euclidean space \mathbb{R}^d , and thus $k \leq d$. The set $\mathcal{U} = \{\mathbf{u}_0, \dots, \mathbf{u}_k\}$ is usually referred to as the vertex set. Moreover, a face of a simplex σ whose vertex set is \mathcal{U} are the simplices based on subsets of \mathcal{U} .

Simplicial complexes are based on simplices of the form (1). Strictly speaking, a simplicial complex $\mathcal{K} \subset \mathbb{R}^n$ is a collection of simplices [*cf.* § 1] that satisfy the conditions: 1) any face of a simplex of \mathcal{K} is a simplex of \mathcal{K} and 2) the intersection of any two simplices of \mathcal{K} is either empty or a common face of the two simplices.

2) *Filtration:* A filtration is a sequence of simplicial complexes $(\mathcal{K}_0, \mathcal{K}_1, \dots)$ that is necessary for generating the intended topological signature. More specifically, a filtration of a simplicial complex \mathcal{K} is a nested sequence of simplicial complexes $\emptyset \subset \mathcal{K}_0 \subset \mathcal{K}_1 \subset \dots \subset \mathcal{K}_m = \mathcal{K}$.

One can build on top of a given point cloud different filtrations, such as Vietoris-Rips (VR), Čech, and Witness [56] among others, which in turn are used to determine the underlying topological structure. We place a major emphasis on the VR filtration since we use it in our subsequent developments. The rule for building the VR complex from the point cloud \mathcal{G} relies on a positive scalar γ . More specifically, given $\gamma > 0$, the VR complex, denoted $V(\mathcal{G}, \gamma)$ with vertex set \mathcal{G} , is defined by the condition

$$[\mathbf{g}_0, \mathbf{g}_1, \dots, \mathbf{g}_n] \in V(\mathcal{G}, \gamma) \iff \|\mathbf{g}_i - \mathbf{g}_j\|_2 \leq \gamma \quad \forall (i, j) \in \{0, \dots, n\}, \quad (2)$$

where $[\mathbf{g}_0, \mathbf{g}_1, \dots, \mathbf{g}_n]$ is a face of $V(\mathcal{G}, \gamma)$, whose vertex set is $\{\mathbf{g}_0, \mathbf{g}_1, \dots, \mathbf{g}_n\} \subset \mathcal{G}$. For $\gamma_0 < \gamma_1 < \dots < \gamma_t$,

$$V(\mathcal{G}, \gamma_0) \subseteq V(\mathcal{G}, \gamma_1) \subseteq \dots \subseteq V(\mathcal{G}, \gamma_t) \quad (3)$$

is held.

3) *PH and PD:* Based on the filtration, how topological features, such as connected components, loops, and voids, appear and disappear can be computed. These are essentially *structural* properties of the underlying point cloud \mathcal{G} . Loosely speaking, the machinery for computing such topological features and their evolution over different spatial resolutions γ of the filtration is called PH. PH gives rise to PH groups, one for each non-negative integer p , denoted by \mathcal{H}_p . For example, 1-dimensional PH group \mathcal{H}_1 tracks the evolution of loops that appear in the filtration process. Associated with PH of a point cloud is the PD, a topological signature that summarizes the evolution of the topological features. The horizontal axis of PD corresponds to the birth time of topological features and the vertical axis represents the death time. Hence, PD \mathcal{S} is a multi-set of points in the open halfplane that represent the births (in x -dimension) and deaths (in y -dimension) of all homology classes.

One can define a metric on the space of PDs for solving ML tasks. In this work, we measure the distance between two PDs \mathcal{S}_1 and \mathcal{S}_2 by using the bottleneck distance defined as

$$W(\mathcal{S}_1, \mathcal{S}_2)_\infty = \inf_{\eta: \mathcal{S}_1 \rightarrow \mathcal{S}_2} \sup_{s \in \mathcal{S}_1} \|s - \eta(s)\|_\infty, \quad (4)$$

where η ranges over all bijections \mathcal{S}_1 to \mathcal{S}_2 .

C. Learning PD Vectorizations

Despite the potential of using PDs in ML applications, the space of PDs faces several challenges. For instance, different PDs can contain varying numbers of points, and basic operations, such as addition and scalar multiplication, are not well-defined in the space of PDs [19]. This makes it challenging to use standard vector space operations in the space of PDs, which are integral to many deep learning (DL) algorithms.

To overcome these challenges, we leverage notions from topological data analysis (TDA), seeking vectorization methods to associate a set of PDs with a set of vectors [19], [22].

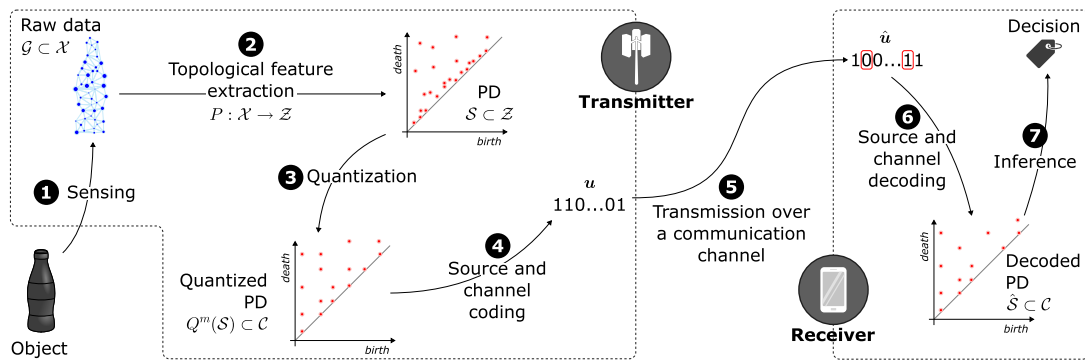


Fig. 1: System model highlighting different stages.

Among these methods, we utilize PersLay, a neural network layer for learning PD vectorizations [19]. Given a PD \mathcal{S} , the PersLay is defined through the following equation:

$$\text{PersLay}(\mathcal{S}) \triangleq \text{op}(\{w(\mathbf{s})\phi(\mathbf{s})\}_{\mathbf{s} \in \mathcal{S}}), \quad (5)$$

where op is a permutation invariant operation, $w : \mathbb{R}^2 \rightarrow \mathbb{R}$ is a weight function for the PD, and $\phi : \mathbb{R}^2 \rightarrow \mathbb{R}^n$ is a representation function that maps each point of the PD to a vector.

III. SYSTEM MODEL AND PROBLEM STATEMENT

We consider a point-to-point communication setting consisting of a transmitting node (TX) acting as a sensor and a receiving node (RX) operating as a decision-maker, cf. Figure 1. TX has point cloud observations over a raw observation space, denoted as \mathcal{X} , which will be referred to as raw data hereinafter. Given any raw data observation $\mathcal{G} \subset \mathcal{X}$ associated with an object (e.g., an image), instead of sharing \mathcal{G} or a compression thereof, TX first transforms \mathcal{G} into a semantic space \mathcal{Z} to yield a PD \mathcal{S} through a mapping $P : \mathcal{X} \rightarrow \mathcal{Z}$ where specific *structural characteristics* of the raw data \mathcal{G} are extracted, cf. stage 1 of Figure 1. More specifically, we consider \mathcal{Z} to be the space on which PDs or in other words, topological summaries of \mathcal{G} are supported. Thus, \mathcal{Z} is simply the open halfplane given by $\mathcal{Z} = \{s = (b, d) \mid b < d\} \subset \mathbb{R}^2$. In the sequel, we refer to topological summaries of the form $P(\mathcal{G}) = \mathcal{S} \subset \mathcal{Z}$ as *PD semantics*. Then TX transmits respective PD semantics to RX over a communication channel.

Upon reception of the PD semantics, RX solely relies on $\mathcal{S} \subset \mathcal{Z}$ for inference. We assume that the downstream task depends upon the output of an inference machinery whose inputs are subsets of \mathcal{Z} carrying structural information of the raw data \mathcal{G} , cf. Figure 1. The inference machinery is trained and deployed at RX². More specifically, we consider a NN classifier as our inference machinery based on the framework of PersLay cf. § II-C.

It is worth noting that, communicating PD semantics \mathcal{S} instead of raw data \mathcal{G} enables an effective representation of the underlying structure of the raw data, yielding an efficient use of the communication channel. As such, we consider a

sequence of raw data $\{\mathcal{G}_i\}_{i \in \mathbb{N}}$, that is mapped by TX to yield a sequence of PD semantics $\{\mathcal{S}_i\}_{i \in \mathbb{N}}$, which in turn are communicated to RX, where $\mathcal{S}_i = P(\mathcal{G}_i)$ for all i . Given the sequence $\{\mathcal{G}_i\}_{i \in \mathbb{N}}$ of raw data and corresponding sequence $\{\mathcal{S}_i\}_{i \in \mathbb{N}}$ of PD semantics, we consider the following problems:

- P1** How to transmit PD semantics and quantify their associated semantic distortions and semantic information rate?
- P2** What trade-offs exist between semantic distortion and the semantic rate?
- P3** What trade-offs exist between semantic distortion and inference accuracy?
- P4** What trade-offs exist between inference accuracy and semantic rate?
- P5** What are the implications of such trade-offs from a design point of view?

Our approach is to glean insights and understanding into the above problems through the use of simple, instructive arguments, and models. Subsequent formulations in § IV and § V provide bases for much of our developments for the problem **P1** above. These developments, together with the inference machinery, characterize the trade-offs and their implications [cf. problems **P2-P5**] as discussed in § VI.

IV. TRANSMISSION OF PD SEMANTICS

We start by recalling that a PD is a multiset supported on the open halfplane \mathcal{Z} cf. § III. Given an arbitrary raw data \mathcal{G} from an application domain under consideration, let $\mathcal{S} = \{s_1, \dots, s_{N_S}\}$ denote the corresponding PD, where N_S represents the number of topological features captured during the filtration process, cf. § II-B2. Thus, the problem of transmitting PD semantics is directly linked with the problem of transmitting each element s_n , $n \in \{1, \dots, N_S\}$, of \mathcal{S} , which are simply vectors in \mathbb{R}^2 . To this end, we consider the application of uniform 2-dimensional (2D) vector quantization similar to high-rate entropy-coded quantization [57, § 3.5]. Though adopting more sophisticated schemes such as vector quantization based on the Lloyd–Max algorithm can be easily carried out, it is beyond the scope of this work, and thus, excluded from the analysis.

A. Quantization of PD Semantics

Note that the set \mathcal{S}_i itself is the semantics that carries structural properties of a given raw data \mathcal{G}_i . Since the elements

²Even though we consider PDs as data for training the inference machinery, we must be careful to choose a suitable notion of semantics for our end-task.

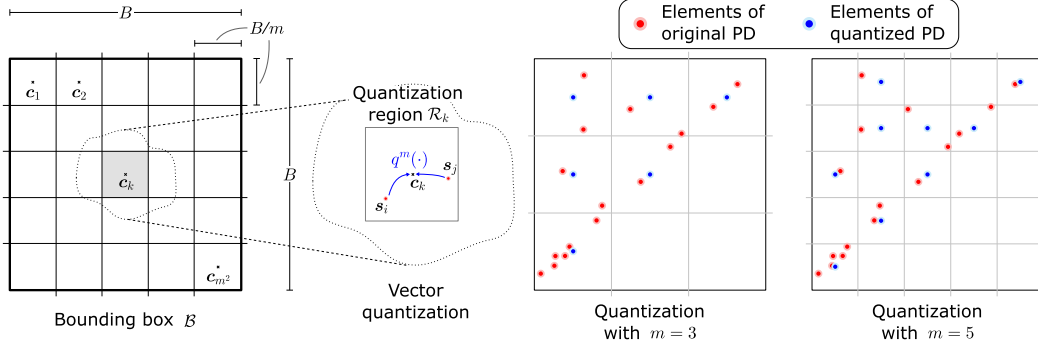


Fig. 2: Uniform 2D vector quantization.

of \mathcal{S}_i are vectors in the nonnegative orthant \mathbb{R}_+^2 , we model the semantic input to the quantizer as a sequence of 2D analog random variables. In particular, the input to the quantizer will be $\{\mathcal{S}_i\}_{i \in \mathbb{N}}$, where $\mathcal{S}_i = \{s_{i,1}, \dots, s_{i,N_{\mathcal{S}_i}}\}$ is the PD semantics of raw data \mathcal{G}_i , $s_{i,j} \in \mathbb{R}^2$, and $N_{\mathcal{S}_i}$ is a finite integer specific to \mathcal{S}_i . Moreover, the elements of \mathcal{S}_i for all i are assumed to be independent, identically distributed (IID) according to a compactly supported probability density function $f_s : \mathbb{R}^2 \rightarrow \mathbb{R}$. Thus, we have the following assumption about the elements of \mathcal{S}_i .

Assumption 1: Elements of \mathcal{S}_i for all i are uniformly bounded. That is, there exists a finite B such that for all i ,

$$\max_{n \in \{1, \dots, N_{\mathcal{S}_i}\}} \|s_{i,n}\|_\infty \leq B.$$

Note that from a practical point of view, the above assumption is not a restriction. For example, it is common in almost all applications that the raw data \mathcal{G}_i is compact. This in turn enables one to come up with a positive scalar $\gamma_t \geq B$ [cf. (3)] beyond which no further topological features will appear, and thus \mathcal{Z} becomes compact.

For all i and $j \in \{1, \dots, N_{\mathcal{S}_i}\}$, the quantizer maps the elements $s_{i,j}$ of \mathcal{S}_i , which are random vectors in \mathbb{R}^2 into discrete 2D random vectors $q_{i,j}$, so that the set \mathcal{C} of representation points for each $q_{i,j}$ is a finite set with cardinality m^2 , i.e., $q_{i,j} \in \mathcal{C} = \{c_1, \dots, c_{m^2}\}$, cf. Figure 2. In particular, the semantic space \mathcal{Z} is enclosed inside the box $\mathcal{B} = \{\mathbf{b} \in \mathbb{R}^2 \mid [0 \ 0]^T \leq \mathbf{b} \leq [B \ B]^T\}$, and each side of the box is divided into m equal intervals. We refer to m as the *bins per dimension* considered for quantization. Consequently, \mathcal{B} is split into m^2 identical and mutually exclusive square-shaped regions. The square-shaped regions are simply the *quantization regions*, which we denote by \mathcal{R}_k , $k \in \{1, \dots, m^2\}$. Let \mathcal{R} be the set of quantization regions, i.e., $\mathcal{R} = \{\mathcal{R}_1, \dots, \mathcal{R}_{m^2}\}$. The geometrical centers of the quantization regions in \mathcal{R} are considered to be the *representation points* c_k , $k \in \{1, \dots, m^2\}$. Formally, given PD semantics $\mathcal{S} = \{s_1, \dots, s_{N_{\mathcal{S}}}\}$, a finite sequence of analog 2D vectors in \mathcal{Z} , the quantizer is viewed as a map $Q^m : \otimes_{n=1}^{N_{\mathcal{S}}} \mathbb{R}^2 \rightarrow \otimes_{n=1}^{N_{\mathcal{S}}} \mathbb{R}^2$ that takes as input the set \mathcal{S} and outputs a set of discrete 2D vectors in \mathcal{C} given by

$$Q^m(\mathcal{S}) = \{q^m(s_1), \dots, q^m(s_{N_{\mathcal{S}}})\}, \quad (6)$$

where $q^m : \mathbb{R}^2 \rightarrow \mathbb{R}^2$ is a 2D vector quantizer defined as

$$s \in \mathcal{R}_k \implies q^m(s) = c_k. \quad (7)$$

Here, the superscript m is used to indicate the number of bins per dimension considered for the quantization.

B. Transmission of PD Semantics and Reconstruction at the Receiver

The representation points c_k , $k \in \{1, \dots, m^2\}$ are mapped into an m^2 -symbol alphabet $\mathcal{A} = \{1, \dots, m^2\}$, which in turn enables the transmitter to communicate PD semantics through a classic digital communication system cf. Figure 1 [57, § 3]. In particular, given an observation \mathcal{S} , symbols from the alphabet \mathcal{A} that correspond to the quantized PD semantics $Q^m(\mathcal{S})$ are encoded into binary digits yielding the related sequence \mathbf{u} of binary symbols, cf. stage 4 of Figure 1. The sequence \mathbf{u} is transmitted by TX to RX through the available communication channel, cf. stage 5 of Figure 1.

At the receiver, the received binary sequence $\hat{\mathbf{u}}$ symbols are converted back to the corresponding 2D representation points in \mathcal{C} to yield the corresponding received PD semantics $\hat{\mathcal{S}}$ of the originally observed PD \mathcal{S} for all $i \in \mathbb{N}$, cf. stage 6 of Figure 1. Note that \mathbf{u} and $\hat{\mathbf{u}}$ are not necessarily identical unless the communication between TX and RX is perfect.

V. PD-SEMANTIC DISTORTION AND RATE

In this section, we quantify the distortion and rate of PD semantics. The purpose is to use them as a basis for subsequent empirical evaluations of the trade-offs, cf. § III. Finally, analogous definitions for AE and raw data are also used in the empirical evaluations as a benchmark.

A. PD-Semantic Distortion

Given a quantization map Q^m over the semantic space \mathcal{Z} [cf. §IV-A], let us next give a simple definition for the resulting semantic distortion due to quantization. The definition for distortion denoted $D_{\text{MSE}}^{\text{PD}}$ is inspired by the notion of classic mean-squared error (MSE) and is given by

$$D_{\text{MSE}}^{\text{PD}} = \mathbb{E}_{f_s} \|s - q^m(s)\|^2 \quad (8)$$

$$= \int_{\mathcal{B}} f_s(s) \|s - q^m(s)\|_2^2 ds \quad (9)$$

$$= \sum_{k=1}^{m^2} \int_{\mathcal{R}_k} f_s(\mathbf{s}) \|\mathbf{s} - \mathbf{c}_k\|_2^2 d\mathbf{s}, \quad (10)$$

where the expectation is taken with respect to the distribution f_s . The superscript indicates that PD semantics are used in the computation.

It is worth pointing out that distortions can also be associated with the PD semantics $\mathcal{S} = \{\mathbf{s}_1, \dots, \mathbf{s}_{N_S}\}$. In such a setting, not only \mathbf{s}_i s, but also N_S is modeled as a random variable, *cf.* Appendix A.

B. PD-Semantic Rate

We start by defining a notion of semantic information within the quantization setting given in § IV. More specifically, semantic information is quantified by considering the entropy of the output of the quantizer q^m [*cf.* (7)]. In particular, we define by p_k the probability of \mathbf{s} residing in region \mathcal{R}_k , i.e.,

$$p_k = \int_{\mathcal{R}_k} f_s(\mathbf{s}) d\mathbf{s}, \quad k = 1, \dots, m^2. \quad (11)$$

Consequently, the entropy H of the quantizer q^m is given by

$$H(q^m) = - \sum_{k=1}^{m^2} p_k \log_2 p_k, \quad (12)$$

where the unit is in bits per symbol and the symbols are chosen from the alphabet \mathcal{A} , *cf.* § IV-B. Finally, we define the rate of PD semantics as R^{PD} [bits/object], where

$$R^{\text{PD}} = M_S H(q^m). \quad (13)$$

Note that $M_S = m(m+1)/2$ and is introduced since p_k is nonzero only for M_S quantization regions, *cf.* Figure 2. This is a direct consequence of f_s being zero over quantization regions lying in the right-bottom triangular space of \mathcal{B} , which follows from the definition of PDs *cf.* § II-B3.

C. Rate and Distortion Definitions for AE based latent representations

For comparison, we have also considered an AE, whose latent dimension is $2d$, where $d \in \mathbb{N}$. As a result, for a given raw data \mathcal{G}_i , the corresponding AE-latent representation denoted \mathcal{A}_i^d , is given by $\mathcal{A}_i^d = \{\mathbf{a}_{i,1}, \dots, \mathbf{a}_{i,d}\}$, where $\mathbf{a}_{i,j} \in \mathbb{R}^2$. In other words, the raw data \mathcal{G}_i is mapped into a set \mathcal{A}_i^d of 2D points whose cardinality is d .

The developments and definitions considered in § IV, § V-A, and § V-B, are applied in the same manner, except that \mathcal{S}_i is replaced by \mathcal{A}_i^d , $N_{\mathcal{S}_i}$ is replaced by $N_{\mathcal{A}_i^d}$, f_s is replaced by f_a^d , and M_S is replaced by M_A . Note that we have $N_{\mathcal{A}_i^d} = d$ for all i . Moreover, the 2D points in the latent representations \mathcal{A}_i^d for all i are assumed to be distributed according to the density function $f_a^d : \mathbb{R}^2 \rightarrow \mathbb{R}$. Note that M_A is the number of quantization regions in which the respective probabilities are nonzero, *cf.* (11). It is worth pointing out that, unlike the case with PD semantics where f_s is guaranteed to be zero over explicit regions in \mathcal{B} , f_a^d is not necessarily zero in any explicit region. Therefore, we have $M_A = m^2$. Furthermore, without loss of generality, we can choose \mathcal{B} in Assumption 1

to be the same even with the latent representations $\{\mathcal{A}_i^d\}_{i \in \mathbb{N}}$, since the latent space can be uniformly scaled and translated.

Finally, the resulting distortion definition for the AE-latent representations is denoted by $D_{\text{MSE}}^{\text{AE},d}$. Moreover, the corresponding data rate is denoted by $R^{\text{AE},d}$.

D. Rate and Distortion Definitions for Raw Data

Analogously, developments and definitions related to the raw data are derived and outlined below without further details since they are clear from the context. The sequence of raw data $\{\mathcal{G}_i\}_{i \in \mathbb{N}}$ is considered with the cardinality of \mathcal{G}_i being $N_{\mathcal{G}_i}$. The density function is denoted by f_g . The number of quantization regions is denoted by M_G which equals m^2 similar to the case of M_A .

As such, the resulting distortion definition for raw data is denoted by $D_{\text{MSE}}^{\text{raw}}$. Moreover, the corresponding data rate for raw data is denoted by R^{raw} .

VI. EMPIRICAL CHARACTERIZATION OF TRADE-OFFS AND THEIR IMPLICATIONS

We are now ready to characterize the underlying trade-offs in terms of PD-semantic distortion $D_{\text{MSE}}^{\text{PD}}$, PD-semantic rate R^{PD} , and inference accuracy which we denote by A^{PD} , *cf.* problems **P2-P5** in § III. Recall that the distortions of AE-latent representations and raw data are denoted by $D_{\text{MSE}}^{\text{AE},d}$ and $D_{\text{MSE}}^{\text{raw}}$, and the respective rates are denoted by $R^{\text{AE},d}$ and R^{raw} , respectively, *cf.* § V-C, § V-D. We further denote by $A^{\text{AE},d}$ and A^{raw} the inference accuracy of AE-latent representations and raw data based systems, respectively. The empirical setup is based on a point cloud dataset based on the MNIST [58], *cf.* § VI-A. Finally, we outline the training and testing environments [§ VI-B] followed by the empirical results [§ VI-C].

A. Dataset and Preprocessing

Note that the proposed developments are generally applied to point cloud data. Therefore, we first create our point cloud dataset based on MNIST [58] which comprises images (objects) of handwritten digits with a size of 28×28 pixels. Given an image from the dataset, each pixel coordinate of the image is modeled by an integer pair (x, y) , where (x, y) is an element of the grid $\{(x, y) \in \mathbb{N}^2 \mid 1 \leq x, y \leq 28\} \subset \mathbb{R}^2$. Using the dataset, we chose a set \mathcal{N} of 600 images and used them throughout our experiments. As a preprocessing step for obtaining realizations of raw random elements \mathcal{G}_i s, we use images in \mathcal{N} . In particular, for each image i in \mathcal{N} , we associate the observation $\mathcal{G}_i = \{(x, y) \mid g^i(x, y) \geq 0.70\}$ ³. Here $g^i : (x, y) \mapsto [-1, 1]$ is the grayscale of the pixel coordinate (x, y) of image i . Thus, we have the finite sequence $\{\mathcal{G}_i\}_{i \in \mathcal{N}}$ of raw data observations. Moreover, the number of classes c for classification is considered to be 3 [i.e., $c = 3$] and is determined by the number of loops of the digits. More specifically, class label j , $j \in \{1, 2, 3\}$ is denoted by \mathcal{C}_j , where $\mathcal{C}_1 = \{0, 6, 9\}$ with each element having one loop, $\mathcal{C}_2 = \{8\}$ with each element having two loops, and $\mathcal{C}_3 = \{1, 2, 3, 4, 5, 7\}$

³For notational simplicity, we use the same notation \mathcal{G}_i and \mathcal{S}_i even when denoting an observation of random \mathcal{G}_i and \mathcal{S}_i , respectively.

with each element having no loops⁴. The number of examples is set to be identical, i.e., 200 per class. The raw dataset $\{\mathcal{G}_i\}_{i \in \mathcal{N}}$ and its corresponding labels are available at [59]. Based on the raw data, together with class labels, we train NN-based classifiers as we discuss next.

B. Training/Testing, and Empirical Computations

Recall that we have the finite sequence $\{\mathcal{G}_i\}_{i \in \mathcal{N}}$ of observations as our raw dataset and corresponding class labels. Associated with each \mathcal{G}_i , we have the corresponding observation \mathcal{S}_i of PD semantics³. For generating AE-latent representations of dimension $2d$, we train a NN model denoted by Enc^d using a commonly used unsupervised training procedure applied to the raw data $\{\mathcal{G}_i\}_{i \in \mathcal{N}}$. Specifically, we have $\text{Enc}^d(\mathcal{G}_i) = \mathcal{A}_i^d$ for all $i \in \mathcal{N}$, see Appendix B. Moreover, we have computed realizations of quantized PD semantics, quantized AE-latent representations, and quantized raw datasets. In particular, for all $i \in \mathcal{N}$, we compute the realizations $\{Q^m(\mathcal{S}_i)\}_{m \in \{10, \dots, 27\}}$ of quantized PD semantics, the realizations $\{Q^m(\mathcal{A}_i^d)\}_{m \in \{10, \dots, 27\}}$ of quantized AE-latent representations, and the realizations $\{Q^m(\mathcal{G}_i)\}_{m \in \{10, \dots, 27\}}$ of quantized raw data⁵ for testing purposes. When training our NN models for classification, we use the sequence of observed PD semantics $\{\mathcal{S}_i\}_{i \in \mathcal{N}}$, corresponding AE-latent representations $\{\mathcal{A}_i^d\}_{i \in \mathcal{N}}$, and the corresponding observations of raw data $\{\mathcal{G}_i\}_{i \in \mathcal{N}}$, together with the class labels.

Our training and testing are based on repeating 2-fold cross-validation [60, § 7.10] over the chosen examples for $T = 25$ times. First, the set of indices $\mathcal{N} = \{1, \dots, 600\}$ is partitioned randomly into a training index set $\mathcal{N}_t^{\text{train}}$ and a testing index set $\mathcal{N}_t^{\text{test}}$ with each having a cardinality of 300. Then, for every $t \in \{1, \dots, T\}$, NN models are trained by considering the sequence of PD semantics $\{\mathcal{S}_i\}_{i \in \mathcal{N}_t^{\text{train}}}$, AE-latent representations $\{\mathcal{A}_i^d\}_{i \in \mathcal{N}_t^{\text{train}}}$, and the sequence of raw data $\{\mathcal{G}_i\}_{i \in \mathcal{N}_t^{\text{train}}}$. The corresponding NN models for classification are denoted by, PD_t , AE_t^d , and Raw_t , where the superscript d signifies that the latent dimension of AE is $2d$. Details of the models are given in Appendix B.

Testing is conducted by using quantized PD semantics, quantized AE-latent representations, and quantized raw data. More specifically, for fixed bins per dimension m , test examples for corresponding quantized PD semantics $\{Q^m(\mathcal{S}_i)\}_{i \in \mathcal{N}_t^{\text{test}}}$ are used with the trained model PD_t for all $t \in \{1, \dots, T\}$. As such, an average inference accuracy \hat{A}^{PD} is computed, which is given by

$$\hat{A}^{\text{PD}} = (1/T) \sum_{t=1}^T A^{\text{PD}}(m, t), \quad (14)$$

where $A^{\text{PD}}(m, t)$ is the average error that corresponds to testing $\{Q^m(\mathcal{S}_i)\}_{i \in \mathcal{N}_t^{\text{test}}}$ with the model PD_t . Similarly, we denote by $\hat{A}^{\text{AE}, d}$ and \hat{A}^{Raw} the average errors that correspond to testing $\{Q^m(\mathcal{A}_i^d)\}_{i \in \mathcal{N}_t^{\text{test}}}$ with AE_t^d models and $\{Q^m(\mathcal{G}_i)\}_{i \in \mathcal{N}_t^{\text{test}}}$ with Raw_t models, respectively.

Note that the probability distribution f_s is not readily available in closed form. Therefore, when computing distortions

⁴We did not consider 4 as a digit with a loop since the dataset consists of handwritten digits. Therefore usually 4 doesn't contain a loop.

⁵The (x, y) -grid of $\mathcal{G}_i \forall i$ is 28×28 . Thus, we let $m \in \{10, \dots, 27\}$.

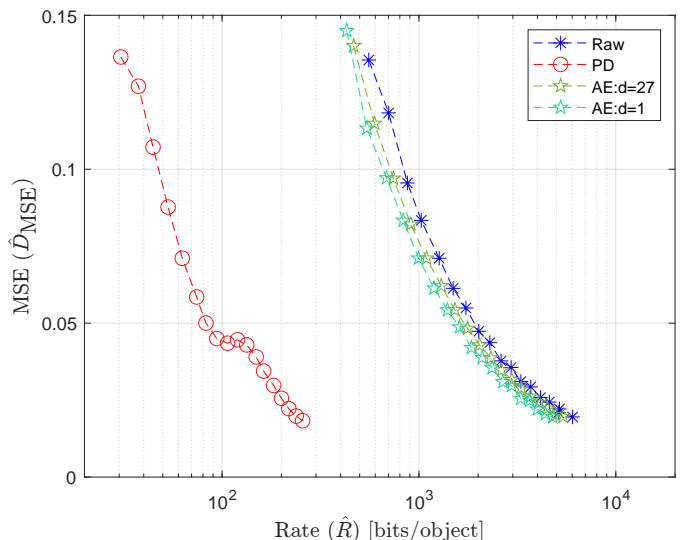


Fig. 3: Empirical trade-off between \hat{D}_{MSE} and \hat{R} .

$D_{\text{MSE}}^{\text{PD}}$ [cf. (8)] and R^{PD} [cf. (11), (12), and (13)], we use an estimate \hat{f}_s of f_s based on the re-scaled histogram of 2D analog vectors $\mathbf{s}_{i,1}, \dots, \mathbf{s}_{i, N_{\mathcal{S}_i}}$ that constitute \mathcal{S}_i for all $i \in \mathcal{N}_t^{\text{test}}$. More specifically, \mathcal{B} is partitioned into 28×28 mutually exclusive boxes with \mathcal{R}_{ab} denoting the (a, b) -th box, and \hat{f}_s supported over \mathcal{B} is given by

$$\hat{f}_s(\mathbf{s}) = \beta \sum_{t=1}^T I_{\mathcal{N}_t^{\text{test}}}(a, b), \quad \mathbf{s} \in \mathcal{R}_{ab}, \quad (15)$$

where $I_{\mathcal{N}_t^{\text{test}}}(i, j)$ is the number of occurrences that $\mathbf{s}_{i,j}$ falls within the region \mathcal{R}_{ab} for some $i \in \mathcal{N}_t^{\text{test}}$ and $j \in \{1, \dots, N_{\mathcal{S}_i}\}$. The scalar β is simply a scaling factor appropriately chosen so that $\int_{\mathcal{B}} \hat{f}_s(\mathbf{s}) d\mathbf{s} = 1$. The resulting numerical values of $D_{\text{MSE}}^{\text{PD}}$ and R^{PD} are denoted by $\hat{D}_{\text{MSE}}^{\text{PD}}$ and \hat{R}^{PD} , respectively. The numerical values $\hat{D}_{\text{MSE}}^{\text{AE}, d}$ and $\hat{R}^{\text{AE}, d}$ of $D_{\text{MSE}}^{\text{AE}, d}$ and $R^{\text{AE}, d}$, respectively, are also computed, by using an estimate \hat{f}_a^d of f_a^d based on the re-scaled histogram of 2D analog vectors $\mathbf{a}_{i,1}, \dots, \mathbf{a}_{i, N_{\mathcal{A}_i^d}}$ that constitute \mathcal{A}_i^d for all $i \in \mathcal{N}$. Empirical evaluations of the distortion $\hat{D}_{\text{MSE}}^{\text{Raw}}$ and the rate \hat{R}^{Raw} corresponding to raw data are analogously computed.

C. Experiments

In this section, we evaluate empirically the trade-offs among distortion D , rate R , and inference accuracy A which are quantified by \hat{D} , \hat{R} , and \hat{A} , respectively. Note that the subscripts and the superscripts in the notation of those entities as we have presented in § VI-B are dropped whenever needed for notational convenience. However, the suitable subscripts and/or superscripts are clear from context. The communication between TX and RX is assumed to be perfect [i.e., error-free] in the simulation considered in § VI-C2 and § VI-C3. Nevertheless, the simulation considered in § VI-C4 assumes imperfect communication between TX and RX.

1) *Trade-offs between Distortion and Rate:* Figure 3 shows the trade-off curves between distortion and rate. In the case of AE-latent representations, the latent dimensions 2 and 54 are considered, i.e., $d = 1$ and $d = 27$. The points of the trade-off

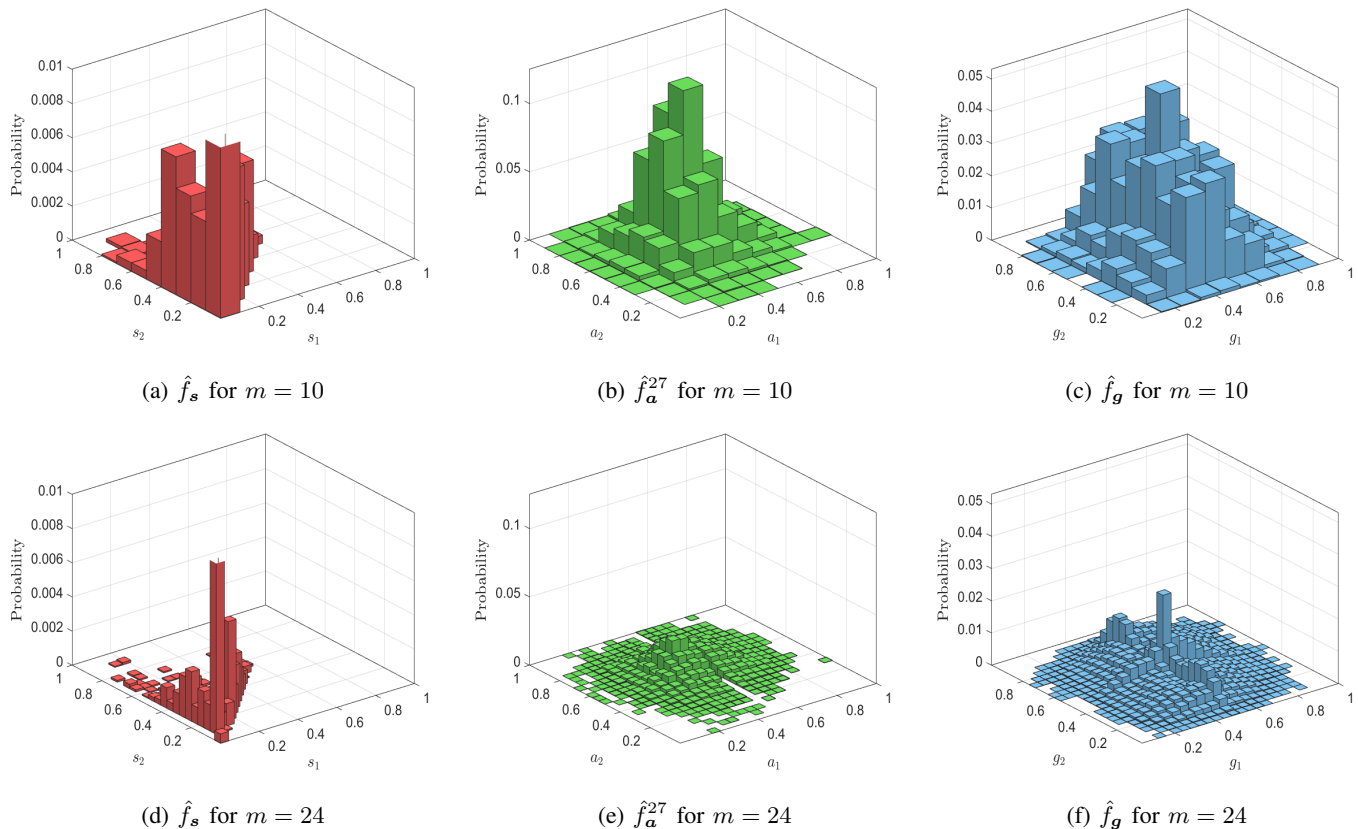


Fig. 4: Empirical probability distributions \hat{f}_s [(a) and (d)], \hat{f}_a^{27} [(b) and (e)], and \hat{f}_g [(c) and (f)] for different m .

curves are obtained by changing the bins per dimension m from 10 to 27.

Figure 3 shows that there is a clear trade-off between distortion D_{MSE} and the rate. Results further show that PD semantics always outperform AE-latent representations and raw data. For example, in the case of PD semantics, roughly a rate of 45 [bits/object] is needed to achieve an MSE of 0.1 while the AE-latent representations and raw require a rate of several hundred [bits/object], roughly 20 times more bits. Moreover, the seemingly constant gap between the curve associated with PD semantics and other curves in Figure 3 indicates that the number of bits required by the others for achieving an MSE specification is simply a constant factor [e.g., $\approx 20 = 13\text{dB}$] times the bits requirement of the case of PD semantics. For example, to achieve an MSE distortion requirement of 0.02, rate requirements are 250 [bits/object] and 5000 [bits/object] for PD semantics and raw data, respectively. Results further show that we receive only a slight benefit in terms of MSE and rates if AE-latent representations are used instead of raw data. Moreover, the smaller the latent dimension, the better the performance of the representations. This is because the trade-off curve corresponding to the smaller d (e.g., $d = 1$) lies below the one corresponding to the larger d (e.g., $d = 27$) even though the differences are not significant.

To get some insight into why the rate requirements of PD semantics are order of magnitude lower than that of both AE-latent representations and raw data, let us plot the

empirical probability distributions \hat{f}_s , \hat{f}_a^d , and \hat{f}_g . Figure 4 depicts empirically computed distributions \hat{f}_s , \hat{f}_a^d and \hat{f}_g for $m \in \{10, 24\}$ according to (15). The empirical distributions show that the probability masses associated with PD semantics are concentrated on a smaller subset of possible outcomes while many with zero or almost zero probability. In contrast, the distributions corresponding to AE-latent representations and raw data are not sparse and the probability masses of the outcomes are more or less comparable in general. Therefore, the results suggest that the uncertainty of PD semantics is lower than that of AE-latent representations and raw data. This is intuitively expected since PDs encode structural properties of the underlying raw data, unlike AE or the raw data itself. As a direct consequence, we see that the rate requirements for transmitting PD semantics are significantly lower than the AE and raw representations.

The preceding observations give important insights into engineering designs to make systems more robust against noise, interference, and fading in practical communication systems. More specifically, the additional bits required in the case of AE-latent representations and raw data can be used in a system based on PD semantics for improving the corresponding MSE. On the other hand, for a given MSE specification, the additional bits required in the case of AE-latent representations and raw data can directly be used in systems that rely on PD semantics to enable the possibility of implementing error detection/correction capabilities yield-

ing more *robustness*. Insights into such advantages of PD semantics over AE-latent representations and raw data under an imperfect communication channel are given in § VI-C4.

2) Trade-offs between Inference Accuracy and Distortion:

Figure 5 shows the empirical trade-off curves between inference accuracy and MSE distortion. The thick curves depict the average results that correspond to trained NN models for classification as discussed in § VI-B [cf. (14)] and the shaded regions highlight their variability. We also plot the trend in thin solid lines as a guideline obtained with function fitting.

Results show that the inference accuracies of models based on raw data tend to deteriorate as MSE distortion increases. In contrast, the inference accuracies of models based on PD semantics and AE-latent representations remain approximately constant, despite the level of MSE, over the considered range. This is indeed an interesting observation from a system design perspective because it demonstrates the advantages of semantics over raw data. As such, this empirical observation suggests that NN models for classification trained with PD semantics and AE-latent representations are more robust than those based on raw data. Results further show that the smaller the latent dimension of AE, the worse the inference accuracy. For example, AE-latent representations with $d = 1$ are clearly inferior to the PD semantic case. However, a higher choice for d can enable AE-latent representations to perform better than PD semantics.

3) Trade-offs between Inference Accuracy and Rate:

It is of practical interest to know how the inference accuracy is changed with rate specifications. Figure 6 shows the trade-off curves between the inference accuracy and the rate. The behavior of the curves is directly dictated by the preceding trade-offs experienced between the distortion and the rate, and those between the inference accuracy and the distortion, cf. Figure 3 and 5.

At first glance, results show that stringent rate specification can only make the inference accuracy worse for NN models based on raw data, cf. blue solid curve. A similar behavior is also evident in the case of AE-latent representations, especially with $d = 27$, even though the deterioration of inference accuracy as the rate decreases is not as significant as in the case of raw data, cf. thick green dashed curve. In contrast, the changes in the rates have an unnoticeable effect on the inference accuracy when the NN models are trained on PD semantics, cf. red solid curves. It is worth highlighting that PD semantics can yield inference accuracies over 80% even with very low rate specifications such as 30.58 [bits/object]. Reasons for such observations are evidenced by the characteristics of probability density \hat{f}_s as depicted in Figure 4.

4) Exploiting Low PD Rates under Imperfect Communications:

Note that the curves depicted in Figure 5 and 6 correspond to settings where the communication between TX and RX is perfect. In contrast, this section considers an imperfect communication between TX and RX. As a representative channel model, the binary symmetric channel (BSC) [61, § 7.1.4] is chosen, cf. stage 5 of Figure 1. BSC complements the input binary symbols with probability $\alpha \in [0, 0.5]$ ⁶, which

⁶The error-free communication channel is a particular case derived when $\alpha = 0$ [cf. § VI-C2 and § VI-C3].

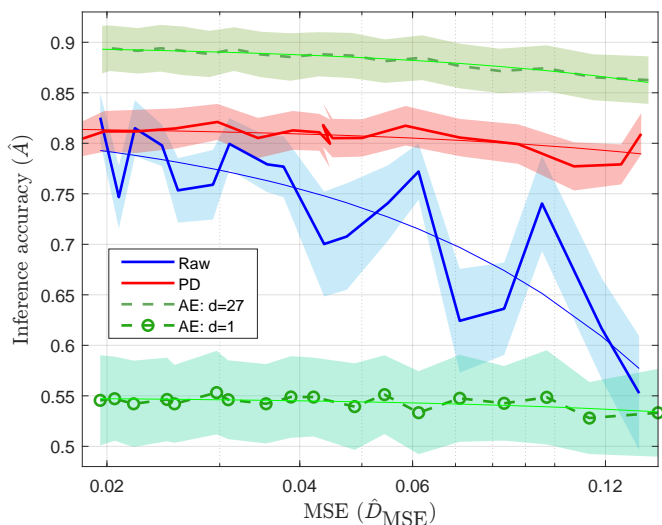


Fig. 5: Empirical trade-off between \hat{A} and \hat{D}_{MSE} .

is referred to as the crossover probability. In this respect, the stage 4 of Figure 1 is implemented in two steps. First, the quantized PD semantics are source-encoded using Huffman codes [61, § 5.8] based on probabilities p_k , $k = 1, \dots, m^2$ [cf. (11), (15)]. Then the resulting source-coded bit stream is channel-coded using $(\bar{n}, \bar{k}, \bar{t})$ -Bose, Chaudhuri, and Hocquenghem (BCH) codes [62, § 6]. Note that, given an $(\bar{n}, \bar{k}, \bar{t})$ -BCH code, \bar{n} denotes the codeword length and \bar{k} denotes the length of binary information digits. The parameter \bar{t} denotes the error correction capability in the sense that the code is capable of correcting all the error patterns of \bar{t} or exhibiting fewer errors.

Before we give any empirical results under imperfect communication channel conditions to compare and contrast PD semantic-based systems with AE-latent representations or raw data-based systems, let us point out meaningful resource settings to provide a fair comparison. First, for AE, we consider the case of $d = 27$ which yields a better inference accuracy. As we noticed in § VI-C3, the inference accuracy of NN models based on PD semantics and AE-latent representations remain almost unchanged over the considered range of rates when the communication is perfect, cf. solid thin red and solid thin green curves in Figure 6. As a result of this robustness of PD semantics and AE-latent representations, designing systems with a coarser quantization, such as $m = 10$, is more suggestive since they account for lower rates. For example, note that the solid red circle and the solid green circle depicted in Figure 6 correspond to *self-information* values of

$$r_{\text{PD}} = 30.58 \quad \text{and} \quad r_{\text{AE}} = 466.19 \quad [\text{bits/object}],$$

respectively on average. On the other hand, if raw data are used in a perfect communication setting, unlike PD semantics, they cannot achieve a similar inference accuracy with a coarser quantization level. Consequently, they have to rely on finer quantization values that account for higher self-information [e.g., $m = 27$], cf. solid blue circle, Figure 6. More specifically, to achieve a better inference accuracy level comparable

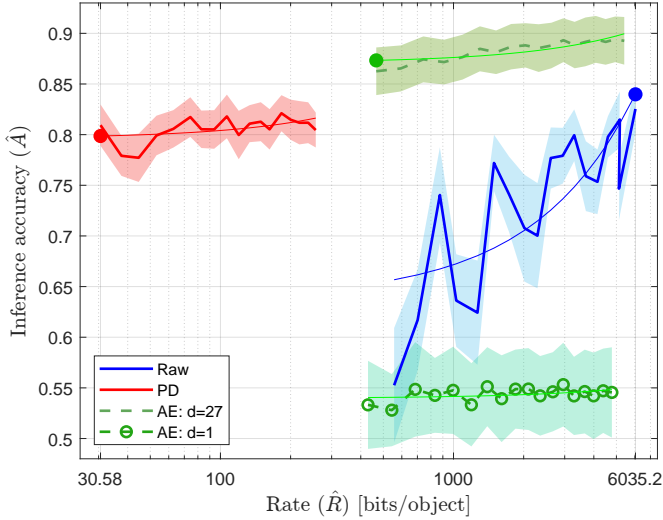


Fig. 6: Empirical trade-off between \hat{A} and \hat{R} .

to PD semantics with r_{PD} [bits/object], the raw data needs to operate with $m = 27$ which corresponds to a rate of

$$r_{Raw} = 6035.20 \quad [\text{bits/object}]$$

on average. These rate limits are depicted by using dotted vertical lines in Figure 7. Thus, from an engineering point of view, the preceding observation can be used as the key to boosting the performance of PD semantic-based systems under imperfect communication settings. As such, in the sequel, we consider a resource setting where no more than r_{Raw} [bits/object] is used ⁷.

A simple calculation suggests that as long as quantized PD semantics is source encoded with an optimal Huffman code ⁸ followed by an $(\bar{n}, \bar{k}, \bar{t})$ -BCH code chosen such that

$$\bar{k} r_{Raw} \geq \bar{n} r_{PD}, \quad (16)$$

the average length of the bit sequence \mathbf{u} per object always remains within the limit r_{Raw} [bits/object]. In our experiments, we let $\bar{n} = 1023$. Therefore, from (16), we have $\bar{k} \geq 5.18$. Thus, all $(1023, \bar{k}, \bar{t})$ -BCH codes with $\bar{k} \geq 6$ operate within the resource limit of r_{Raw} [bits/object]. For example, suppose $\bar{k} = 208$, i.e., the corresponding BCH code is $(1023, 208, 115)$ [62, Table 6.1]. In this case, the actual communication rate requirement to transmit $r_{PD} = 30.58$ information bits is simply 150.41 bits which is indeed less than r_{Raw} . On the other hand, the coded PD semantics become robust under imperfect communication settings since $(1023, 208, 115)$ -BCH code is capable of correcting all error patterns of 115 or fewer errors. As such, the key is to encode quantized PD semantics by using $(1023, \bar{k}, \bar{t})$ -BCH codes whose \bar{k} conforms to (16) with the hope of being more robust against channel impairments. By replacing r_{PD} in (16) by r_{AE} , $(1023, \bar{k}, \bar{t})$ -BCH codes compatible with AE-latent representations that operate within the resource limit r_{Raw} [bits/object] can be computed similarly.

⁷This is the resource requirement of the raw data-based systems to achieve the highest possible inference accuracy in our simulations.

⁸The source rates [cf. (11), (12)] are based on the entropy and thus, we rely on an optimal source code such as Huffman to perform source encoding.

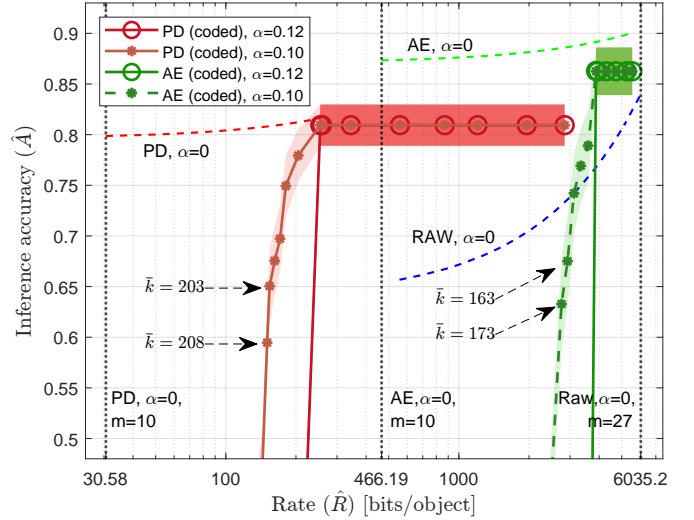


Fig. 7: Empirical trade-off between \hat{A} and \hat{R} (coded). For comparison, the trends of \hat{A} versus rate \hat{R} under perfect communication settings are reported as thin dashed curves.

Figure 7 shows the inference accuracy versus coded information rate requirements for quantized PD semantics and quantized AE-latent representations with $(1023, \bar{k}, \bar{t})$ -BCH codes, where the bins per dimension $m = 10$. Compatible BCH codes used with PD semantics correspond to $\bar{k} = 208, 203, 193, 183, 173, 153, 123, 121, 91, 56, 36, 26, 16$, and 11. On the other hand, compatible BCH codes used with AE-latent representations correspond to $\bar{k} = 173, 163, 153, 143, 133, 123, 111, 101, 91$, and 86. Simulations are conducted for two BSC conditions. In particular, case 1 considers a BSC with $\alpha = 0.12$ and case 2 considers a BSC with $\alpha = 0.1$.

Results show that the best inference accuracy levels of perfect communication settings are also attainable even under the imperfect communication settings when PD semantics are coded with $(1023, \bar{k}, \bar{t})$ -BCH codes. We emphasize that this is achieved without utilizing no more than r_{Raw} [bits/object]. For example, with coded PD semantics, for both $\alpha = 0.1$ and $\alpha = 0.12$, the best inference accuracy is achieved by using $(1023, \bar{k}, \bar{t})$ -BCH codes with $\bar{k} = 123, 121, 91, 56, 36, 26, 16$, and 11 that correspond to coded information rates of 254.35, 258.55, 343.79, 558.66, 869.02, 1203.26, 1955.30, and 2844.08 [bits/object], respectively. Of course, the code $(1023, 123, 170)$ with the lowest resource requirement (i.e., highest code rate), is preferable among those. It is worth pointing out that, such a choice corresponds to more than 23-fold communication resource reduction compared to r_{Raw} [bits/object], even under imperfect communication. Thus, results suggest that when a system based on raw data under perfect communication settings infers one object, a system based on PD semantics will infer 23 objects while maintaining the same order of inference accuracy even under imperfect communication.

Coded AE-latent representations can also yield channel error-free inference accuracy levels with some $(1023, \bar{k}, \bar{t})$ -BCH codes. For example, BCH codes with $\bar{k} =$

133, 123, 111, 101, 91, and 86 that correspond to coded information rates of 3877.38, 3941.47, 4296.55, 4721.96, 5240.85, and 5545.55 [bits/object], yield the best inference accuracy under both BCH channel conditions $\alpha = 0.1$ and $\alpha = 0.12$. Therefore, results show that the rate requirements in coded AE-latent representations are significantly higher compared to the rate requirements of coded PD semantics. For example, the minimum rate requirement of coded PD semantics to operate at an inference accuracy of more than 80% is, roughly, 15 times as small as the rate requirement of coded AE-latent representations. As such, in practice, the choice of PD semantics enables not only withstanding the imperfect communication impairments effectively but also the improvements in the *latency* compared to the choices of both AE-latent representations and raw data.

VII. CONCLUSION

In this work, we explored the advantages of persistence diagrams (PDs) over raw point cloud data as structural semantics for a point-to-point communication setting. The transmitter (e.g., sensor) used PD semantics in its transmissions and the receiver (e.g., central node) carried out inference using the received semantics. We developed qualitative definitions for distortion and rate of PD semantics and quantitatively characterized the trade-offs among the distortion, the rate, and the inference accuracy at the receiver node. Our empirical results demonstrated that PD semantics leads to more effective use of transmission channels, enhanced degrees of freedom for incorporating error detection and correction capabilities, and improved robustness to communication channel imperfections. Results further highlighted the potential of using structural semantics in goal-oriented communication settings ensuring high efficiency and robustness of communication systems, where intrinsic channel impairments, such as noise, interference, and fading are inevitable.

APPENDIX A

A GENERAL DISTORTION DEFINITION FOR \mathcal{S}

Our second notion of semantic distortion is inspired by the bottleneck distance (4). However, the map η in (4) is restricted to be the quantization map Q^m given in (6). More specifically, the distortion of \mathcal{S} , denoted $D_{\text{BN}}^{\text{sem}}$, is given by

$$D_{\text{BN}}^{\text{sem}} = \mathbb{E}_{f_{N_S}} \mathbb{E}_{f_{s_1, \dots, s_{N_S}} | N_S} \left[\max_{i \in \{1, 2, \dots, N_S\}} \|s_i - q^m(s_i)\|_{\infty} \right],$$

where the expectation $\mathbb{E}_{f_{s_1, \dots, s_{N_S}} | N_S}$ is taken with respect to the conditional distribution $f_{s_1, \dots, s_{N_S}} | N_S$ and expectation $\mathbb{E}_{f_{N_S}}$ is taken with respect to the distribution f_{N_S} . A similar notion of distortion can also be constructed for raw data based on $f_{g_1, \dots, g_{N_G}} | N_G$ and f_{N_G} .

The distributions $f_{s_1, \dots, s_{N_S}} | N_S$, f_{N_S} , $f_{g_1, \dots, g_{N_G}} | N_G$, and f_{N_G} are not available in practice and therefore, one must rely on numerical approaches to yield estimates. Assuming s_1, \dots, s_{N_S} (and g_1, \dots, g_{N_G}) are conditionally IID given N_S (and N_G) according to some conditional distribution $f_{s_i | N_S}$ (and $f_{g_i | N_G}$), Figure 8 illustrates the related empirical probability distributions \hat{f}_{N_S} , $\hat{f}_{s_i | N_S}$, \hat{f}_{N_G} , and $\hat{f}_{g_i | N_G}$ for some

choices of m based on what the corresponding distortions can numerically be evaluated.

Note that the sparsity characteristics of the empirical conditional distributions are very similar to those in Figure 4. That is the probability masses of the distributions associated with PD semantics are concentrated on a few outcomes and zero or almost zero for most of the outcomes, unlike the probability masses of conditional distributions that correspond to raw data. Thus, the results suggest that the numerical evaluations of trade-off curves with the general distortion definition behave similarly to those with $D_{\text{MSE}}^{\text{sem}}$.

APPENDIX B

PARAMETERS FOR THE EMPIRICAL SIMULATIONS

For computing PD \mathcal{S}_i from a given raw data \mathcal{G}_i , we employed the VR filtration with a positive scalar $\gamma_t = 16$, cf. (3). Vectorized representations of the PDs were then generated using PersLay, with its parameters defined as follows: $\text{op} := \text{top2}$, $w := \text{PowerPerslayWeight}$, and $\phi := \text{TentPerslayPhi}$, cf. (5). These computations were carried out using the GUDHI library [63].

Our empirical simulations employed NN models, with their parameters summarized in Table I. Moreover, the AEs were trained on raw data $\{\mathcal{G}_i\}_{i \in \mathcal{N}_{26}^{\text{train}}}$ using the binary cross-entropy loss function. The classifiers were trained with the categorical cross-entropy loss function, and all models were optimized using the ADAM optimizer with a learning rate of 0.001.

TABLE I: A summary of the NN models.

Purpose	Model	# of parameters	Library
Training encoders	Enc ²⁷	442566	PyTorch [64]
	Enc ¹	435858	PyTorch
Training classifiers	PD _t	201747	TensorFlow [65]
	Raw _t	201731	PyTorch
	AE _t ²⁷	2339	PyTorch
	AE _t ¹	27	PyTorch

REFERENCES

- [1] C. Shannon and W. Weaver, *The Mathematical Theory of Communication*, ser. Illini books. University of Illinois Press, 1949.
- [2] C. E. Shannon, "A mathematical theory of communication," *The Bell system technical journal*, vol. 27, no. 3, pp. 379–423, 1948.
- [3] R. Carnap and Y. Bar-Hillel, "An outline of a theory of semantic information," *Research Laboratory of Electronics, MIT*, 1952.
- [4] —, "An outline of a theory of semantic information," *Journal of Symbolic Logic*, vol. 19, no. 3, pp. 230–232, 1954.
- [5] Y. Bar-Hillel and R. Carnap, "Semantic information," *The British Journal for the Philosophy of Science*, vol. 4, no. 14, pp. 147–157, 1953.
- [6] Q. Lan, D. Wen, Z. Zhang, Q. Zeng, X. Chen, P. Popovski, and K. Huang, "What is semantic communication? A view on conveying meaning in the era of machine intelligence," *Journal of Communications and Information Networks*, vol. 6, no. 4, pp. 336–371, 2021.
- [7] E. C. Strinati and S. Barbarossa, "6G networks: Beyond Shannon towards semantic and goal-oriented communications," *Computer Networks*, vol. 190, p. 107930, 2021.
- [8] H. Seo, J. Park, M. Bennis, and M. Debbah, "Semantics-native communication via contextual reasoning," *IEEE Transactions on Cognitive Communications and Networking*, vol. 9, no. 3, pp. 604–617, 2023.

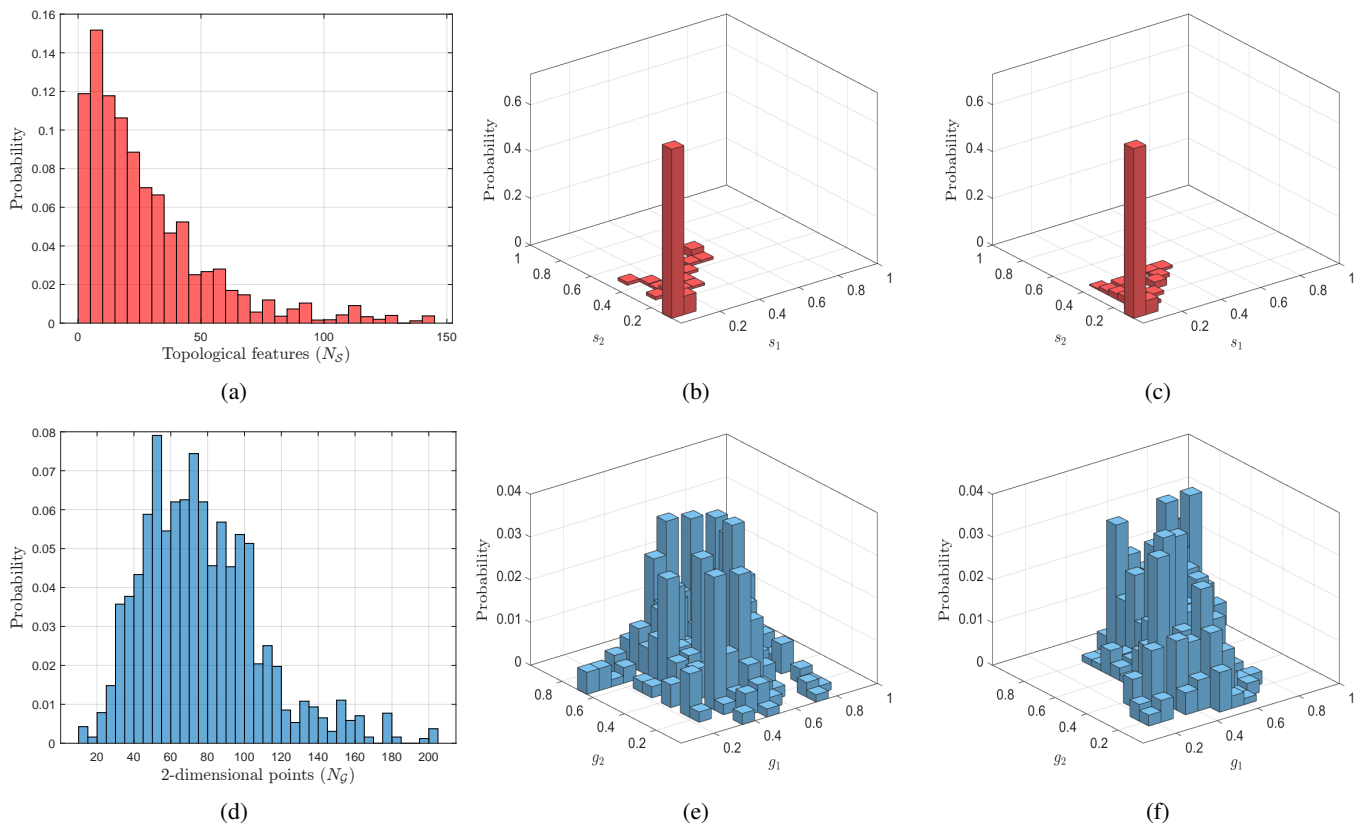


Fig. 8: Empirical probability distributions where s_1, \dots, s_{N_S} (and g_1, \dots, g_{N_G}) are conditionally IID given N_S (and N_G) according to $f_{s|N_S}$ (and $f_{g|N_G}$): (a) \hat{f}_{N_S} , (b) $\hat{f}_{s|N_S=6}$ for $m = 16$, (c) $\hat{f}_{s|N_S=10}$ for $m = 16$, (d) \hat{f}_{N_G} , (e) $\hat{f}_{g|N_G=50}$ for $m = 16$, (f) $\hat{f}_{g|N_G=100}$ for $m = 16$.

- [9] W. Yang, H. Du, Z. Q. Liew, W. Y. B. Lim, Z. Xiong, D. Niyato, X. Chi, X. Shen, and C. Miao, "Semantic communications for future internet: Fundamentals, applications, and challenges," *IEEE Communications Surveys & Tutorials*, vol. 25, no. 1, pp. 213–250, 2022.
- [10] Z. Qin, X. Tao, J. Lu, W. Tong, and G. Y. Li, "Semantic communications: Principles and challenges," *arXiv preprint arXiv:2201.01389*, 2021.
- [11] C. Zhang, H. Zou, S. Lasaulce, W. Saad, M. Kountouris, and M. Bennis, "Goal-oriented communications for the IoT and application to data compression," *IEEE Internet of Things Magazine*, vol. 5, no. 4, pp. 58–63, 2022.
- [12] Z. Lu, R. Li, K. Lu, X. Chen, E. Hossain, Z. Zhao, and H. Zhang, "Semantics-empowered communications: A tutorial-cum-survey," *IEEE Communications Surveys & Tutorials*, 2023.
- [13] D. Gündüz, Z. Qin, I. E. Aguerri, H. S. Dhillon, Z. Yang, A. Yener, K. K. Wong, and C.-B. Chae, "Beyond transmitting bits: Context, semantics, and task-oriented communications," *IEEE Journal on Selected Areas in Communications*, vol. 41, no. 1, pp. 5–41, 2022.
- [14] A. Mostaani, T. X. Vu, S. K. Sharma, V.-D. Nguyen, Q. Liao, and S. Chatzinotas, "Task-oriented communication design in cyber-physical systems: A survey on theory and applications," *IEEE Access*, vol. 10, pp. 133 842–133 868, 2022.
- [15] T. M. Getu, G. Kaddoum, and M. Bennis, "A survey on goal-oriented semantic communication: Techniques, challenges, and future directions," *IEEE Access*, 2024.
- [16] T. Berger, *Rate Distortion Theory: A Mathematical Basis for Data Compression*, ser. Prentice-Hall electrical engineering series. Prentice-Hall, 1971.
- [17] N. Tishby, F. C. Pereira, and W. Bialek, "The information bottleneck method," *arXiv preprint physics/0004057*, 2000.
- [18] F. Chazal and B. Michel, "An introduction to topological data analysis: fundamental and practical aspects for data scientists," *Frontiers in artificial intelligence*, vol. 4, p. 667963, 2021.
- [19] M. Carrière, F. Chazal, Y. Ike, T. Lacombe, M. Royer, and Y. Umeda, "PersLay: A neural network layer for persistence diagrams and new graph topological signatures," in *International Conference on Artificial Intelligence and Statistics*. PMLR, 2020, pp. 2786–2796.
- [20] M. Moor, M. Horn, B. Rieck, and K. Borgwardt, "Topological autoencoders," in *International conference on machine learning*. PMLR, 2020, pp. 7045–7054.
- [21] R. B. Gabriellson, B. J. Nelson, A. Dwaraknath, and P. Skraba, "A topology layer for machine learning," in *International Conference on Artificial Intelligence and Statistics*. PMLR, 2020, pp. 1553–1563.
- [22] K. Kim, J. Kim, M. Zaheer, J. Kim, F. Chazal, and L. Wasserman, "PLay: Efficient topological layer based on persistent landscapes," *Advances in Neural Information Processing Systems*, vol. 33, pp. 15 965–15 977, 2020.
- [23] R. Reinauer, M. Caorsi, and N. Berkouk, "Persformer: A transformer architecture for topological machine learning," *arXiv preprint arXiv:2112.15210*, 2021.
- [24] T. Papamarkou, T. Birdal, M. Bronstein, G. Carlsson, J. Curry, Y. Gao, M. Hajji, R. Kwitt, P. Liò, P. Di Lorenzo *et al.*, "Position paper: Challenges and opportunities in topological deep learning," *arXiv preprint arXiv:2402.08871*, 2024.
- [25] T. Bonis, M. Ovsjanikov, S. Oudot, and F. Chazal, "Persistence-based pooling for shape pose recognition," in *Computational Topology in Image Context: 6th International Workshop, CTIC 2016, Marseille, France, June 15-17, 2016, Proceedings 6*. Springer, 2016, pp. 19–29.
- [26] M. Carrière, M. Cuturi, and S. Oudot, "Sliced Wasserstein kernel for persistence diagrams," in *International conference on machine learning*. PMLR, 2017, pp. 664–673.
- [27] A. Karan and A. Kaygun, "Time series classification via topological data analysis," *Expert Systems with Applications*, vol. 183, p. 115326, 2021.
- [28] T. Lacombe, M. Cuturi, and S. Oudot, "Large scale computation of means and clusters for persistence diagrams using optimal transport," *Advances in Neural Information Processing Systems*, vol. 31, 2018.
- [29] P. Skraba, M. Ovsjanikov, F. Chazal, and L. Guibas, "Persistence-based segmentation of deformable shapes," in *2010 IEEE Computer Society*

- Conference on Computer Vision and Pattern Recognition-Workshops*. IEEE, 2010, pp. 45–52.
- [30] H. Xie, Z. Qin, G. Y. Li, and B.-H. Juang, “Deep learning enabled semantic communication systems,” *IEEE Transactions on Signal Processing*, vol. 69, pp. 2663–2675, 2021.
- [31] Q. Zhou, R. Li, Z. Zhao, C. Peng, and H. Zhang, “Semantic communication with adaptive universal transformer,” *IEEE Wireless Communications Letters*, vol. 11, no. 3, pp. 453–457, 2021.
- [32] S. Wang, J. Dai, Z. Liang, K. Niu, Z. Si, C. Dong, X. Qin, and P. Zhang, “Wireless deep video semantic transmission,” *IEEE Journal on Selected Areas in Communications*, vol. 41, no. 1, pp. 214–229, 2022.
- [33] J. Dai, S. Wang, K. Tan, Z. Si, X. Qin, K. Niu, and P. Zhang, “Nonlinear transform source-channel coding for semantic communications,” *IEEE Journal on Selected Areas in Communications*, vol. 40, no. 8, pp. 2300–2316, 2022.
- [34] R. Torfason, F. Mentzer, E. Agustsson, M. Tschannen, R. Timofte, and L. Van Gool, “Towards image understanding from deep compression without decoding,” *arXiv preprint arXiv:1803.06131*, 2018.
- [35] D. Strouse and D. J. Schwab, “The deterministic information bottleneck,” *Neural computation*, vol. 29, no. 6, pp. 1611–1630, 2017.
- [36] F. Liu, W. Tong, Y. Yang, Z. Sun, and C. Guo, “Task-oriented image semantic communication based on rate-distortion theory,” *arXiv preprint arXiv:2201.10929*, 2022.
- [37] J. Shao, Y. Mao, and J. Zhang, “Learning task-oriented communication for edge inference: An information bottleneck approach,” *IEEE Journal on Selected Areas in Communications*, vol. 40, no. 1, pp. 197–211, 2021.
- [38] S. Xie, S. Ma, M. Ding, Y. Shi, M. Tang, and Y. Wu, “Robust information bottleneck for task-oriented communication with digital modulation,” *IEEE Journal on Selected Areas in Communications*, vol. 41, no. 8, pp. 2577–2591, 2023.
- [39] E. Beck, C. Bockelmann, and A. Dekorsy, “Semantic information recovery in wireless networks,” *Sensors*, vol. 23, no. 14, p. 6347, 2023.
- [40] T. Wu, H. Ren, P. Li, and J. Leskovec, “Graph information bottleneck,” *Advances in Neural Information Processing Systems*, vol. 33, pp. 20 437–20 448, 2020.
- [41] I. E. Aguerri and A. Zaidi, “Distributed variational representation learning,” *IEEE transactions on pattern analysis and machine intelligence*, vol. 43, no. 1, pp. 120–138, 2019.
- [42] Y. Wang, M. Chen, W. Saad, T. Luo, S. Cui, and H. V. Poor, “Performance optimization for semantic communications: An attention-based learning approach,” in *2021 IEEE Global Communications Conference (GLOBECOM)*. IEEE, 2021, pp. 1–6.
- [43] Q. Wang, Z. Mao, B. Wang, and L. Guo, “Knowledge graph embedding: A survey of approaches and applications,” *IEEE transactions on knowledge and data engineering*, vol. 29, no. 12, pp. 2724–2743, 2017.
- [44] S. Ji, S. Pan, E. Cambria, P. Marttinen, and S. Y. Philip, “A survey on knowledge graphs: Representation, acquisition, and applications,” *IEEE transactions on neural networks and learning systems*, vol. 33, no. 2, pp. 494–514, 2021.
- [45] F. Zhou, Y. Li, X. Zhang, Q. Wu, X. Lei, and R. Q. Hu, “Cognitive semantic communication systems driven by knowledge graph,” in *ICC 2022-IEEE International Conference on Communications*. IEEE, 2022, pp. 4860–4865.
- [46] Y. Xiao, Y. Li, G. Shi, and H. V. Poor, “Reasoning on the air: An implicit semantic communication architecture,” in *2022 IEEE International Conference on Communications Workshops (ICC Workshops)*. IEEE, 2022, pp. 289–294.
- [47] Q. Zhao, H. Zou, M. Bennis, M. Debbah, E. Almazrouei, and F. Bader, “Joint semantic-native communication and inference via minimal simplicial structures,” in *GLOBECOM 2023-2023 IEEE Global Communications Conference*. IEEE, 2023, pp. 2233–2238.
- [48] Q. Zhao, M. Bennis, M. Debbah, and D. B. Da Costa, “Semantic-native communication: A simplicial complex perspective,” in *2022 IEEE Globecom Workshops (GC Wkshps)*. IEEE, 2022, pp. 1513–1518.
- [49] C. K. Thomas and W. Saad, “Neuro-symbolic artificial intelligence (ai) for intent based semantic communication,” in *GLOBECOM 2022-2022 IEEE Global Communications Conference*. IEEE, 2022, pp. 2698–2703.
- [50] E. Uysal, O. Kaya, A. Ephremides, J. Gross, M. Codreanu, P. Popovski, M. Assaad, G. Liva, A. Munari, B. Soret *et al.*, “Semantic communications in networked systems: A data significance perspective,” *IEEE Network*, vol. 36, no. 4, pp. 233–240, 2022.
- [51] G. Gan, C. Ma, and J. Wu, *Data clustering: theory, algorithms, and applications*. SIAM, 2020.
- [52] C. M. Bishop and N. M. Nasrabadi, *Pattern recognition and machine learning*. Springer, 2006, vol. 4, no. 4.
- [53] E. Davis, “Logical formalizations of commonsense reasoning: a survey,” *Journal of Artificial Intelligence Research*, vol. 59, pp. 651–723, 2017.
- [54] B. Schölkopf, F. Locatello, S. Bauer, N. R. Ke, N. Kalchbrenner, A. Goyal, and Y. Bengio, “Toward causal representation learning,” *Proceedings of the IEEE*, vol. 109, no. 5, pp. 612–634, 2021.
- [55] H. Edelsbrunner and J. L. Harer, *Computational topology: an introduction*. American Mathematical Society, 2022.
- [56] V. De Silva and G. E. Carlsson, “Topological estimation using witness complexes,” in *PBG*, 2004, pp. 157–166.
- [57] R. G. Gallager *et al.*, *Principles of digital communication*. Cambridge University Press Cambridge, UK, 2008, vol. 1.
- [58] L. Deng, “The MNIST database of handwritten digit images for machine learning research,” *IEEE Signal Processing Magazine*, vol. 29, no. 6, pp. 141–142, 2012.
- [59] ICON, “Data-for-structural-semantics-using-tda,” <https://github.com/ICONgroupCWC/Data-for-Structural-Semantics-using-TDA.git>, 2024.
- [60] T. Hastie, R. Tibshirani, J. H. Friedman, and J. H. Friedman, *The elements of statistical learning: data mining, inference, and prediction*. Springer, 2009, vol. 2.
- [61] T. M. Cover and J. A. Thomas, *Elements of Information Theory (Wiley Series in Telecommunications and Signal Processing)*. USA: Wiley-Interscience, 2006.
- [62] S. Lin and D. J. Costello, *Error Control Coding*, 2nd ed. Pearson Prentice Hall, 2004.
- [63] The GUDHI Project, *GUDHI User and Reference Manual*, 3.1.1 ed. GUDHI Editorial Board, 2020. [Online]. Available: <https://gudhi.inria.fr/doc/3.1.1/>
- [64] A. Paszke, S. Gross, F. Massa, A. Lerer, J. Bradbury, G. Chanan, T. Killeen, Z. Lin, N. Gimelshein, L. Antiga *et al.*, “Pytorch: An imperative style, high-performance deep learning library,” *Advances in neural information processing systems*, vol. 32, 2019.
- [65] M. Abadi, A. Agarwal, P. Barham, E. Brevdo, Z. Chen, C. Citro, G. S. Corrado, A. Davis, J. Dean, M. Devin *et al.*, “Tensorflow: Large-scale machine learning on heterogeneous systems,” 2015.